

Generation of spectrally uncorrelated biphotons via fibernonlinear quantum interference

Zhengtong Wei(卫正统), Chuan Qu(瞿川), Tian'an Wu(吴天安), Yuanyuan Li(李媛媛), Bo Li(李博), and Shenghai Zhang(张胜海)

Citation: Chin. Phys. B, 2023, 32 (**6**): 064202. DOI: 10.1088/1674-1056/acb767
Journal homepage: http://cpb.iphy.ac.cn; http://iopscience.iop.org/cpb

What follows is a list of articles you may be interested in

Enhanced phase sensitive amplification towards improving noise immunity

Hui Guo(郭辉), Zhi Li(李治), Hengxin Sun(孙恒信), Kui Liu(刘奎), and Jiangrui Gao(郜江瑞)
Chin. Phys. B, 2023, 32 (**5**): 054204. DOI: 10.1088/1674-1056/acbdeb

Effective dynamics and quantum state engineering by periodic kicks

Zhi-Cheng Shi(施志成), Zhen Chen(陈阵), Jian-Hui Wang(王建辉), Yan Xia(夏岩), and X X Yi(衣学喜)
Chin. Phys. B, 2023, 32 (**4**): 044210. DOI: 10.1088/1674-1056/ac7bfc

Quantum properties of nonclassical states generated by an optomechanical system with catalytic quantum scissors

Heng-Mei Li(李恒梅), Bao-Hua Yang(杨保华), Hong-Chun Yuan(袁洪春), and Ye-Jun Xu(许业军)
Chin. Phys. B, 2023, 32 (**1**): 014202. DOI: 10.1088/1674-1056/ac7206

Heralded path-entangled NOON states generation from a reconfigurable photonic chip

Xinyao Yu(于馨瑶), Pingyu Zhu(朱枰谕), Yang Wang(王洋), Miaomiao Yu(余苗苗), Chao Wu(吴超),Shichuan Xue(薛诗川), Qilin Zheng(郑骑林), Yingwen Liu(刘英文), Junjie Wu(吴俊杰), and Ping Xu(徐平)
Chin. Phys. B, 2022, 31 (**6**): 064203. DOI: 10.1088/1674-1056/ac3501

Different supercontinuum generation processes in photonic crystal fibers pumped with a 1064-nm picosecond pulse

Chen Hong-Wei (谌鸿伟), Jin Ai-Jun (靳爱军), Chen Sheng-Ping (陈胜平), Hou Jing (侯静), Lu Qi-Sheng (陆启生)
Chin. Phys. B, 2013, 22 (**8**): 084205. DOI: 10.1088/1674-1056/22/8/084205

Generation of spectrally uncorrelated biphotons via fiber nonlinear quantum interference

Zhengtong Wei(卫正统), Chuan Qu(瞿川), Tian'an Wu(吴天安),
Yuanyuan Li(李媛媛), Bo Li(李博), and Shenghai Zhang(张胜海)†

College of Basic Department, Information Engineering University, Zhengzhou 450000, *China*

(Received 5 December 2022; revised manuscript received 18 January 2023; accepted manuscript online 31 January 2023)

Spectrally uncorrelated biphotons are the essential resources for achieving various quantum information processing protocols. We theoretically investigate the generation of spectrally uncorrelated biphotons emitted by spontaneous four-wave mixing from a fiber nonlinear interferometer which consists of an N-stage nonlinear gain fiber and an $(N-1)$-stage dispersion modulation fiber. The output biphoton states of nonlinear interference are the coherent superposition of various biphoton states born in each nonlinear fiber, and thus the interference fringe will reshape the biphoton joint spectra. As a result, resorting to Taylor expansion to first order for phase mismatching, we theoretically verify that the orientation of phase matching contours will rotate in a specific way with only varying the length of dispersion modulation fiber. The rotation in orientation of phase matching contours may result in spectrally uncorrelated biphotons and even arbitrary correlation biphotons. Further, we choose micro/nanofiber as the nonlinear gain fiber and single-mode communication fiber as dispersion modulation fiber to numerically simulate the generation of spectrally uncorrelated biphotons from spontaneous fourwave mixing. Here, due to significant frequency detuning (hundreds of THz), Raman background noise can be considerably suppressed, even at room temperature, and photons with largely tunable wavelengths can be achieved, indicating a practicability in many quantum fields. A photon mode purity of 97.2% will be theoretically attained without weakening the heralding nature of biphoton sources. We think that this fiber nonlinear interference with the flexibly engineered quantum state can be an excellent practical source for quantum information processing.

Keywords: photon mode purity, nonlinear quantum interference, group velocity matching

PACS: 42.50.Dv, 42.50.Ex, 42.65.Lm, 42.81.–i **DOI:** 10.1088/1674-1056/acb767

1. Introduction

Single photons and biphotons are the prominent carriers for quantum information processing (QIP),[1] which typically requires specific properties, particularly, uncorrelated spectra, also known as spectrally pure states. Spectrally uncorrelated biphotons are the essential elements in achieving high visibility of quantum interference,[2,3] which yields a high operation fidelity and a high probability of success for several QIP protocols such as quantum teleportation,[4] quantum key distribution,[5] and linear optical quantum computing.[6] Up to now, heralding single photons or biphotons from spontaneous parametric processes, mainly referring to spontaneous parametric down conversion (SPDC)[7,8] and spontaneous four-wave mixing (SFWM),[9] are the most economic and effective photon sources. In order to obtain precise time synchronization with respect to photon arrival and to attain higher pump peak power, pulsed lasers are selected as pump. However, due to broadband nature of pump pulsed lasers and strict phase matching condition in a dispersion nonlinear medium, the photons generated from these processes are of complicated frequency correlation and temporal multi-mode nature. The most common approach to obtain spectrally uncorrelated biphotons is to reshape the spectrum with narrow-band filters, but this method will degrade the brightness and weaken the heralding nature of biphoton source. In addition, a more sophisticated way for combating this issue is to engineer the spectrum of spontaneous parametric processes, where the group velocity matching (GVM) is achieved.[8,10] However, GVM crucially depends on the dispersion exhibited by the nonlinear materials and tends to occur only in specific wavelength ranges.[11,12]

The phase matching of spontaneous parametric processes depends on dispersion characteristic of the nonlinear gain material, such that engineering dispersion may affect GVM and further leads to spectrally uncorrelated biphotons. Therefore, a nonlinear interferometer (NLI) can be used to engineer quantum state. N-stage NLI, consisting of N-stage nonlinear gain medium with one piece dispersion modulation medium between every adjacent two, has applications in dispersion compensation of optical parametric amplifier,[13–16] precision phase measurement beyond standard quantum limit,[17–19] super-resolution spectroscopy and imaging[20,21] and biphoton spectrum shaping.[22] Cui *et al.*[23–25] have demonstrated that the spectrally uncorrelated biphotons can be obtained via fiber NLI, therein dispersion-shifted fiber as nonlinear gain medium and single mode fiber as dispersion modulation medium in a small frequency detuning case. However, due to the immovability in zero-dispersion wavelength of dispersion-shifted fiber, the spectrally pure biphotons can only be obtained around 1550 nm.

Therefore, we further analytically investigate the phe-

†Corresponding author. E-mail: Ccstshz@163.com

© 2023 Chinese Physical Society and IOP Publishing Ltd

nomenon that fiber NLI leads to the rotation of phase matching contours, indicating the feasibility of spectrally uncorrelated biphotons and even arbitrary correlation biphotons. Micro/nanofiber (MNF) is optical fiber with diameters close to subwavelength or nanometer scale.[26] Indeed, due to small mode area and field enhancement originated from the tight confinement, the efficiency of SFWM enhances significantly in MNF. We present a practical scheme of fiber NLI, therein MNF as nonlinear gain medium and single-mode communication fiber as dispersion modulation medium to generate spectrally uncorrelated biphotons. Here, spectrally uncorrelated biphotons are generated from SFWM in the significant frequency detuning (hundreds of THz) cases. Thus, photons with largely tunable wavelengths can be achieved, and Raman background noise can be considerably suppressed.

In this paper, we first introduce the theory of biphotons and its mode purity dependent on Schmidt decomposition. We give the GVM condition for generating spectrally uncorrelated biphotons. Then, we present a structure of N-stage fiber NLI and give a specific form of its output state. In addition, we analytically investigate the underlying reasons, for which NLI leads to the rotation of phase matching contours, and further verify it by numerical simulation. For a significant frequency detuning case, we numerically simulate the generation of spectrally uncorrelated biphotons from SFWM in fiber NLI, therein MNF as nonlinear gain medium and single-mode communication fiber as dispersion modulation medium.

2. Spectrally uncorrelated biphotons

In general, ignoring multiphoton, we can present the output quantum state of spontaneous parametric process as follows:[27,28]

$$|\Psi\rangle \approx |\mathrm{vac}\rangle + \eta\,|\Psi_2\rangle\,, \tag{1}$$

where η is a constant related to conversion efficiency, and $|\Psi_2\rangle$ refers to biphoton states with a form of

$$|\Psi_2\rangle = \int \mathrm{d}\omega_\mathrm{s}\,\mathrm{d}\omega_\mathrm{i}\mathcal{F}(\omega_\mathrm{s},\omega_\mathrm{i})\hat{a}_\mathrm{s}^\dagger(\omega_\mathrm{s})\hat{a}_\mathrm{i}^\dagger(\omega_\mathrm{i})|\mathrm{vac}\rangle. \tag{2}$$

In the above expression, $|\mathrm{vac}\rangle$ refers to vacuum state, $\hat{a}_\mathrm{s}^\dagger(\omega_\mathrm{s})$ and $\hat{a}_\mathrm{i}^\dagger(\omega_\mathrm{i})$ are the creation operators of the signal and idler fields in nonlinear fiber spatial mode at ω_s and ω_i, respectively, and $\mathcal{F}(\omega_\mathrm{s},\omega_\mathrm{i})$ is the joint spectral amplitude function (JSA), which reveals the spectral entanglement properties of biphotons. Here,

$$\begin{aligned}\mathcal{F}(\omega_\mathrm{s},\omega_\mathrm{i}) = &\int \mathrm{d}\omega\mathcal{E}_1(\omega)\mathcal{E}_2(\omega_\mathrm{s}+\omega_\mathrm{i}-\omega)\\ &\times\mathrm{sinc}\left[\frac{L}{2}\Delta\beta(\omega,\omega_\mathrm{s},\omega_\mathrm{i})\right]\\ &\times\exp\left[\mathrm{i}\frac{L}{2}\Delta\beta(\omega,\omega_\mathrm{s},\omega_\mathrm{i})\right],\end{aligned} \tag{3}$$

where $\mathcal{E}_\mu$ ($\mu = 1,\ 2$) is pump spectral amplitudes for two pumps, L is the length of nonlinear fiber, and $\Delta\beta$ is the phase mismatch. Further, the squared absolute value of the function $|\mathcal{F}(\omega_\mathrm{s},\omega_\mathrm{i})|^2$, known as joint spectral intensity (JSI), describes the probability density of the photon pair generation as a function of the frequencies. In the case that the four participating photons are linearly co-polarized, $\Delta\beta$ is given by

$$\begin{aligned}\Delta\beta(\omega,\omega_\mathrm{s},\omega_\mathrm{i}) = &\ \beta(\omega)+\beta(\omega_\mathrm{s}+\omega_\mathrm{i}-\omega)-\beta(\omega_\mathrm{s})\\ &-\beta(\omega_\mathrm{i})-(\gamma_1P_1+\gamma_2P_2),\end{aligned} \tag{4}$$

where β is the propagation constant and the last term is self/cross-phase modulation contribution given in terms of nonlinear parameters γ_μ and pump peak powers P_μ ($\mu = 1,\ 2$).[27] For degenerate Gaussian pump, we know $\mathcal{E}_1(\omega) = \mathcal{E}_2(\omega)$ and both of them in the formation of Gaussian function. Then, using the linear approximation, Eq. (3) can be rewritten as the product of pump envelope functions $\mathcal{E}(\omega)$ and the phase matching function $\mathcal{P}(\omega_\mathrm{s},\omega_\mathrm{i})$, i.e.,[10,29]

$$\mathcal{F}(\omega_\mathrm{s},\omega_\mathrm{i}) = \mathcal{E}(\omega_\mathrm{s},\omega_\mathrm{i})\mathcal{P}(\omega_\mathrm{s},\omega_\mathrm{i}) \tag{5}$$

with

$$\mathcal{E}(\omega_\mathrm{s},\omega_\mathrm{i}) = E_{\mathrm{p}0}\exp\left[-\frac{(\omega_\mathrm{s}+\omega_\mathrm{i}-2\omega_{\mathrm{p}0})^2}{4\sigma_\mathrm{p}^2}\right], \tag{6}$$

$$\mathcal{P}(\omega_\mathrm{s},\omega_\mathrm{i}) = \mathrm{sinc}\left[\frac{L}{2}\Delta\beta(\omega_\mathrm{s},\omega_\mathrm{i})\right]\exp\left[\mathrm{i}\frac{L}{2}\Delta\beta(\omega_\mathrm{s},\omega_\mathrm{i})\right], \tag{7}$$

where $\Delta\beta(\omega_\mathrm{s},\omega_\mathrm{i}) = 2\beta[(\omega_\mathrm{s}+\omega_\mathrm{i})/2]-\beta(\omega_\mathrm{s})-\beta(\omega_\mathrm{i})-2\gamma P$, $\gamma_1 = \gamma_2 = \gamma$, $P_1 = P_2 = P$.

Spectrally uncorrelated biphoton sources are characterized by $\mathcal{F}(\omega_\mathrm{s},\omega_\mathrm{i}) = \mathcal{S}(\omega_\mathrm{s})\mathcal{I}(\omega_\mathrm{i})$, for which $\mathcal{S}(\omega_\mathrm{s})$ and $\mathcal{I}(\omega_\mathrm{i})$ depend only on ω_s and ω_i, respectively. Typically, the purity of single photons can be quantified via the Schmidt decomposition of the JSA[30]

$$\mathcal{F}(\omega_\mathrm{s},\omega_\mathrm{i}) = \sum_k r_k\mathcal{S}_k(\omega_\mathrm{s})\mathcal{I}_k(\omega_\mathrm{i}), \tag{8}$$

where mode expansion coefficients read $r_k \geq 0$ and $\sum_k r_k^2 = 1$, and two sets of orthonormal functions read $\{\mathcal{S}(\omega_\mathrm{s}),\mathcal{I}(\omega_\mathrm{i})\}$. The Schmidt mode number is $K = 1/\sum_k r_k^4$, and the purity of single photons is equal to $1/K$. Using first-order Taylor expansion of $\beta(\omega_\mu)$ at $\omega_{\mu0}$ where perfect phase-matching is attained ($\mu = \mathrm{p,\ s,\ i}$), phase mismatch can be approximately given by

$$\Delta\beta \approx \tau_\mathrm{s}\Omega_\mathrm{s} + \tau_\mathrm{i}\Omega_\mathrm{i}, \tag{9}$$

where $\tau_{\mathrm{s(i)}} = \beta_{\mathrm{p}0}^{(1)} - \beta_{\mathrm{s(i)}0}^{(1)}$ with $\beta_j^{(1)} = \mathrm{d}\beta(\omega)/\mathrm{d}\omega|_{\omega_j}$ ($j = \mathrm{p}0,\ \mathrm{s}0,\ \mathrm{i}0$) is the so-called group velocity mismatch, $\Omega_\mathrm{s} = \omega_\mathrm{s} - \omega_{\mathrm{s}0}$, and $\Omega_\mathrm{i} = \omega_\mathrm{i} - \omega_{\mathrm{i}0}$. In addition, the phase matching angle θ_s, i.e., the angle between perfect phase matching curve and ω_s axis in $\{\omega_\mathrm{s},\omega_\mathrm{i}\}$ space, is given by $\theta_\mathrm{s} = -\arctan(\tau_\mathrm{s}/\tau_\mathrm{i})$. In order to analytically obtain the condition for generating spectrally uncorrelated biphotons, we apply the approximation

$\mathrm{sinc}(x) \approx \exp[-(ax)^2]$ ($a = 0.439$), so that the simplified JSA is written as

$$\begin{aligned}\mathcal{F}(\Omega_\mathrm{s},\Omega_\mathrm{i}) &= \exp\left[-\frac{(\Omega_\mathrm{s}+\Omega_\mathrm{i})^2}{4\sigma_\mathrm{p}^2}\right]\times\mathrm{sinc}\left[\frac{(\tau_\mathrm{s}\Omega_\mathrm{s}+\tau_\mathrm{i}\Omega_\mathrm{i})L}{2}\right]\\ &= \exp\left[\left(\frac{1}{4\sigma_\mathrm{p}^2}+\frac{a^2L^2\tau_\mathrm{s}^2}{4}\right)\Omega_\mathrm{s}^2\right.\\ &\quad-\left(\frac{1}{4\sigma_\mathrm{p}^2}+\frac{a^2L^2\tau_\mathrm{i}^2}{4}\right)\Omega_\mathrm{i}^2\\ &\quad\left.-\left(\frac{1}{2\sigma_\mathrm{p}^2}+\frac{a^2L^2\tau_\mathrm{s}\tau_\mathrm{i}}{2}\right)\Omega_\mathrm{s}\Omega_\mathrm{i}\right]. \qquad (10)\end{aligned}$$

Obviously, the condition to eliminate the cross term of Ω_s and Ω_i is

$$\frac{1}{\sigma_\mathrm{p}^2}+a^2L^2\tau_\mathrm{s}\tau_\mathrm{i}=0, \qquad (11)$$

which implies that only if $\tau_\mathrm{s}\tau_\mathrm{i}<0$ is fulfilled, can an appropriate pump or length of nonlinear fiber be chosen to achieve the factorable JSA.[31] In particular, the case of $\tau_\mathrm{s}=-\tau_\mathrm{i}$ is defined as symmetric group velocity matching (SGVM). Alternatively, the case of $\tau_\mathrm{s}=0$ or $\tau_\mathrm{i}=0$ with a very broad bandwidth pump enables Eq. (11) to be appropriately fulfilled, which is defined as the asymmetric group velocity matching (AGVM).

3. Fiber nonlinear interference

As shown above, GVM in Eq. (11) is a powerful technique to generate the spectrum uncorrelation biphotons. Nevertheless, GVM crucially depends on the dispersion exhibited by the nonlinear materials and tends to occur only in specific wavelength ranges. Here, we propose a fiber NLI scheme, as shown in Fig. 1, to achieve GVM flexibly, in principle, at arbitrary phase matching wavelengths of nonlinear fiber. The N-stage nonlinear interference consists of N-piece nonlinear fiber (NLF) and $(N-1)$-piece dispersion modulation fiber (DMF). It is further assumed that each NLF has length L^NL, while each DMF has length L^DM. Therefore, the DMF-induced phase mismatch, analogous to SFWM, is given by

$$\Delta k(\omega_\mathrm{s},\omega_\mathrm{i}) = 2k(\omega_\mathrm{p})-k(\omega_\mathrm{s})-k(\omega_\mathrm{i}), \qquad (12)$$

where k is the propagation constant in DMF.

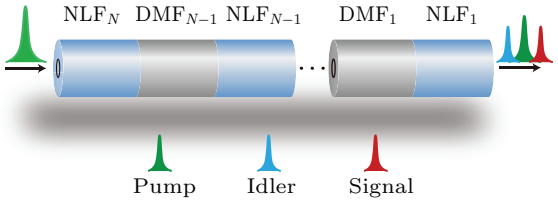


Fig. 1. Schematic of N-stage fiber nonlinear interference consisting of N-piece nonlinear fiber and $(N-1)$-piece dispersion modulation fiber.

Under the assumption of neglecting all transmission losses, the output biphoton states of nonlinear interference are the coherent superposition of various biphoton states born in each NLF, such that the output biphoton states have a form of

$$\begin{aligned}|\Psi^\mathrm{NLI}\rangle &= |\Psi^{(1)}\rangle+|\Psi^{(2)}\rangle+\cdots+|\Psi^{(N)}\rangle\\ &= \left[1+\mathrm{e}^{\mathrm{i}\Phi}+\mathrm{e}^{\mathrm{i}2\Phi}+\cdots+\mathrm{e}^{\mathrm{i}(N-1)\Phi}\right]|\Psi^{(1)}\rangle\\ &= |\mathrm{vac}\rangle+\eta\int \mathrm{d}\omega_\mathrm{s}\,\mathrm{d}\omega_\mathrm{i}\mathcal{F}^\mathrm{NLI}(\omega_\mathrm{s},\omega_\mathrm{i})\,|\omega_\mathrm{s},\omega_\mathrm{i}\rangle \qquad (13)\end{aligned}$$

with

$$\Phi=\Delta\beta(\omega_\mathrm{s},\omega_\mathrm{i})L^\mathrm{NL}+\Delta k(\omega_\mathrm{s},\omega_\mathrm{i})L^\mathrm{DM} \qquad (14)$$

and the JSA of the output biphotons

$$\begin{aligned}\mathcal{F}^\mathrm{NLI}(\mathrm{s},,\omega_\mathrm{i}) &= \mathcal{F}(\omega_\mathrm{s},\omega_\mathrm{i})\,\mathcal{M}(\varphi)\\ &= \mathcal{E}(\omega_\mathrm{s},\omega_\mathrm{i})\,[\mathcal{P}(\omega_\mathrm{s},\omega_\mathrm{i})\mathcal{M}(\varphi)], \qquad (15)\end{aligned}$$

where $\varphi=\Phi/2$ and

$$\mathcal{M}(\varphi)=1+\sum_{k=1}^{N-1}\mathrm{e}^{\mathrm{i}k\Phi}=\frac{\sin(N\varphi)}{\sin\varphi}\,\mathrm{e}^{\mathrm{i}(N-1)\varphi}. \qquad (16)$$

Indeed, $\mathcal{M}(\varphi)$ is the modulation function analogous to interference term in a classical optics interferometer. Here, $\mathcal{M}(\varphi)$ modifies the phase matching function of biphotons to $\mathcal{P}^\mathrm{NLI}(\omega_\mathrm{s},\omega_\mathrm{i})=\mathcal{P}(\omega_\mathrm{s},\omega_\mathrm{i})\mathcal{M}(\varphi)$. As depicted in Fig. 2, $|\mathcal{M}(\varphi)|$ exhibits a periodic structure of narrow peaks that are separated by π, with $N-2$ vice peaks between adjacent prominent peaks. The centers of prominent peaks coincide with each other for various N, then the width of the peak diminishes with increasing N.

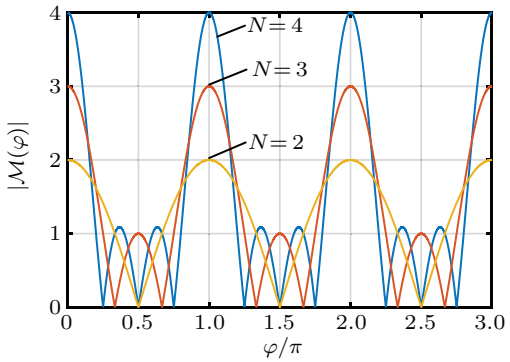


Fig. 2. Plots of $|\mathcal{M}(\varphi)|$ versus φ for various N.

Likewise, expanding φ to first-order Taylor series at the perfectly phase-matched frequencies of ω_p0, ω_s0, and ω_i0, respectively, φ is approximatively given by

$$\begin{aligned}\varphi &\approx \frac{1}{2}(\tau_\mathrm{s}^\mathrm{NL}\Omega_\mathrm{s}+\tau_\mathrm{i}^\mathrm{NL}\Omega_\mathrm{i})L^\mathrm{NL}\\ &\quad+\frac{1}{2}(\tau_\mathrm{s}^\mathrm{DM}\Omega_\mathrm{s}+\tau_\mathrm{i}^\mathrm{DM}\Omega_\mathrm{i})L^\mathrm{DM}+\frac{k_0}{2}L^\mathrm{DM}\\ &= \frac{1}{2}L^\mathrm{NL}(\tau_\mathrm{s}^\mathrm{NL}+\xi\tau_\mathrm{s}^\mathrm{DM})\Omega_\mathrm{s}\\ &\quad+\frac{1}{2}L^\mathrm{NL}(\tau_\mathrm{i}^\mathrm{NL}+\xi\tau_\mathrm{i}^\mathrm{DM})\Omega_\mathrm{i}+\frac{k_0}{2}L^\mathrm{DM}, \qquad (17)\end{aligned}$$

where $\tau_{\mathrm{s(i)}}^\mathrm{DM}=k_\mathrm{p0}^{(1)}-k_\mathrm{s(i)0}^{(1)}$ with $k_j^{(1)}=\mathrm{d}k(\omega)/\mathrm{d}\omega|_{\omega_j}$ ($j=\mathrm{p0},\mathrm{s0},\mathrm{i0}$) is group velocity mismatch in DMF and $\tau_{\mathrm{s(i)}}^\mathrm{NL}=\beta_\mathrm{p0}^{(1)}-\beta_\mathrm{s(i)0}^{(1)}$

with $\beta_j^{(1)} = \mathrm{d}\beta(\omega)/\mathrm{d}\omega|_{\omega_j}$ (j = p0, s0, i0) is group velocity mismatch in NLF, $k_0 = 2k(\omega_{\mathrm{p0}}) - k(\omega_{\mathrm{s0}}) - k(\omega_{\mathrm{i0}})$ is a constant, and $\xi = L^{\mathrm{DM}}/L^{\mathrm{NL}}$ ($\xi > 0$). Remarkably, Cui *et al.*[24,30,32] revealed that the contour of $|\mathcal{M}(\varphi)|$ has an appearance of periodic parallel stripes, such that the orientation angle of phase matching may vary to (0, $\pi/2$) and further achieve GVM. Consequently, amounting to phase matching curve, the orientation angle of these stripes, which is the angle between connection lines of $|\mathcal{M}(\varphi)|$ peaks and ω_{s}-axis in $\{\omega_{\mathrm{s}}, \omega_{\mathrm{i}}\}$ space, is determined by the first-order dispersion

$$\tan(\theta^{\mathrm{NLI}}) = -\frac{\tau_{\mathrm{s}}^{\mathrm{NL}} + \xi\tau_{\mathrm{s}}^{\mathrm{DM}}}{\tau_{\mathrm{i}}^{\mathrm{NL}} + \xi\tau_{\mathrm{i}}^{\mathrm{DM}}}. \tag{18}$$

Further, Eq. (18) can be rewritten as

$$\tan(\theta^{\mathrm{NLI}}) = -\frac{\frac{\tau_{\mathrm{s}}^{\mathrm{NL}}}{\tau_{\mathrm{i}}^{\mathrm{NL}}} - \frac{\tau_{\mathrm{s}}^{\mathrm{DM}}}{\tau_{\mathrm{i}}^{\mathrm{DM}}}}{1 + \xi\frac{\tau_{\mathrm{i}}^{\mathrm{DM}}}{\tau_{\mathrm{i}}^{\mathrm{NL}}}} - \frac{\tau_{\mathrm{s}}^{\mathrm{DM}}}{\tau_{\mathrm{i}}^{\mathrm{DM}}}. \tag{19}$$

Evidently, it suggests that $\tan(\theta^{\mathrm{NLI}})$ will vary from $\tau_{\mathrm{s}}^{\mathrm{NL}}/\tau_{\mathrm{i}}^{\mathrm{NL}}$ to $\tau_{\mathrm{s}}^{\mathrm{DM}}/\tau_{\mathrm{i}}^{\mathrm{DM}}$ with ξ varying from 0 to ∞, indicating that the orientation of phase matching will rotate in a specific way. Concretely, we investigate this rotation process through the various combinations for the values of $\tau_{\mathrm{s}}^{\mathrm{NL}}/\tau_{\mathrm{i}}^{\mathrm{NL}}$, $\tau_{\mathrm{s}}^{\mathrm{DM}}/\tau_{\mathrm{i}}^{\mathrm{DM}}$, and $\tau_{\mathrm{i}}^{\mathrm{DM}}/\tau_{\mathrm{i}}^{\mathrm{NL}}$, as shown in Fig. 3. The x-axis and y-axis just represent the signs of $\tau_{\mathrm{s}}^{\mathrm{NL}}/\tau_{\mathrm{i}}^{\mathrm{NL}}$ and $\tau_{\mathrm{i}}^{\mathrm{DM}}/\tau_{\mathrm{i}}^{\mathrm{NL}}$, respectively, not concrete quantity. Therefore, it is easy to realize the GVM, for which, intuitively, the arrow rotates to the first or third quadrant by only extending the length of DMFs.

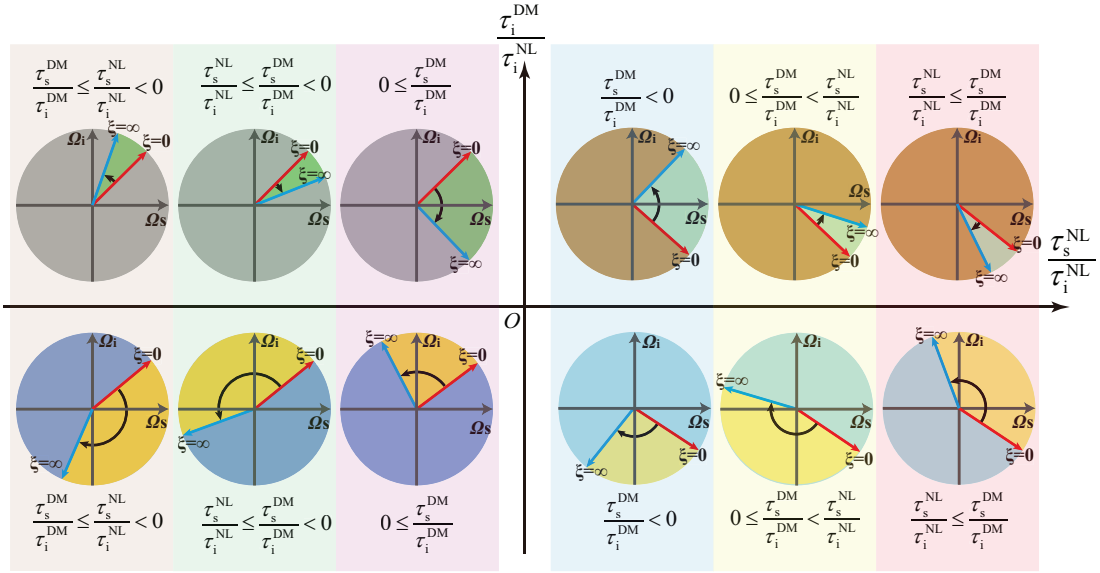


Fig. 3. Rotation in orientation of phase matching contours in terms of various combinations of $\tau_{\mathrm{s}}^{\mathrm{NL}}/\tau_{\mathrm{i}}^{\mathrm{NL}}$, $\tau_{\mathrm{s}}^{\mathrm{DM}}/\tau_{\mathrm{i}}^{\mathrm{DM}}$, and $\tau_{\mathrm{i}}^{\mathrm{DM}}/\tau_{\mathrm{i}}^{\mathrm{NL}}$. The wavelengths are corresponding to the perfectly phase-matched wavelengths of SFWM in nonlinear gain fiber.

4. Rotation of phase matching contours

As for numerical simulation, we choose MNF as the NLF corresponding to a significant frequency detuning case. Due to small mode area and field enhancement originating from the tight confinement, the nonlinear effect enhances significantly in MNF. Shukhin *et al.* experimentally demonstrated that the bright single photon sources can be generated by degenerate SFWM in MNF.[33,34] The signal photons are in fiber telecommunication O-band which enables efficient transmission, while idler photons are in near visible light which has a high detection efficiency. Firstly, we numerically investigate the properties of biphoton JSA for SFWM in MNF. In general, the MNF is fabricated from the standard single mode fibers by using heating and stretching method,[35,36] where the radius profile of MNF can be divided as two zones, a uniform waist region in the middle and two bilaterally symmetric tapered regions.[33,37] In addition, MNF pigtail remains standard single mode fiber, indicating a low connection and transmission loss. The shape of tapered regions is in a form of exponential function, which can be characterized by a parameter α ($-1 < \alpha < 1$), with a larger α corresponding to a steeper slope. The radius of tapered regions is given by

$$r(z) = \begin{cases} r_0\,\mathrm{e}^{-\frac{z}{u}}, & \alpha = 0, \\ r_0\left[1 + \frac{2\alpha z}{(1-\alpha)u}\right]^{-\frac{1}{2\alpha}}, & \alpha \neq 0, \end{cases} \tag{20}$$

where r_0 is the initial radius and u is the length of waist region.

Noticeably, while the phase matching function will alter due to the presence of tapered region, the pump envelope function remains unchanged. In order to calculate the JSA of biphotons, the overall MNF, including waist region and tapered region, is divided by the T cross sections into several parts whose length are all Λ, hence the total phase-matching function is the superposition of those calculated for each cross section[27]

$$\mathcal{P}(\omega_{\mathrm{s}}, \omega_{\mathrm{i}}) = \sum_{m=1}^{T}\left[\mathrm{sinc}\left(\frac{\Delta\beta_m\Lambda}{2}\right)\exp\left(\frac{\mathrm{i}\Delta\beta_m\Lambda}{2}\right)\right.$$

$$\times \exp\left(\mathrm{i}\sum_{n=m+1}^{T}\Delta\beta_n\Lambda\right)g_m\Bigg], \tag{21}$$

where g_m is related to SFWM nonlinear coefficient of mth section. It can be written as

$$g_m = \frac{1}{\int \mathrm{d}x \int \mathrm{d}y f_{m,\mathrm{p}}^2(x,y) f_{m,\mathrm{s}}^*(x,y) f_{m,\mathrm{i}}^*(x,y)}, \tag{22}$$

with $f_{m,(j)}(x,y)$ $(j = \mathrm{p},\ \mathrm{s},\ \mathrm{i})$ denoting the transverse spatial distribution in the process of SFWM in mth section. Here, we numerically simulate the JSA of biphotons with the MNF configurations of 0.85 μm in diameter, 3 cm in waist region length and $\alpha = 0.5$, and the pump configurations of 1006 nm in central wavelength and 0.5 nm in spectral width. We show the phase matching function, pump envelope function, and JSI in Figs. 4(a), 4(b), and 4(c), respectively.

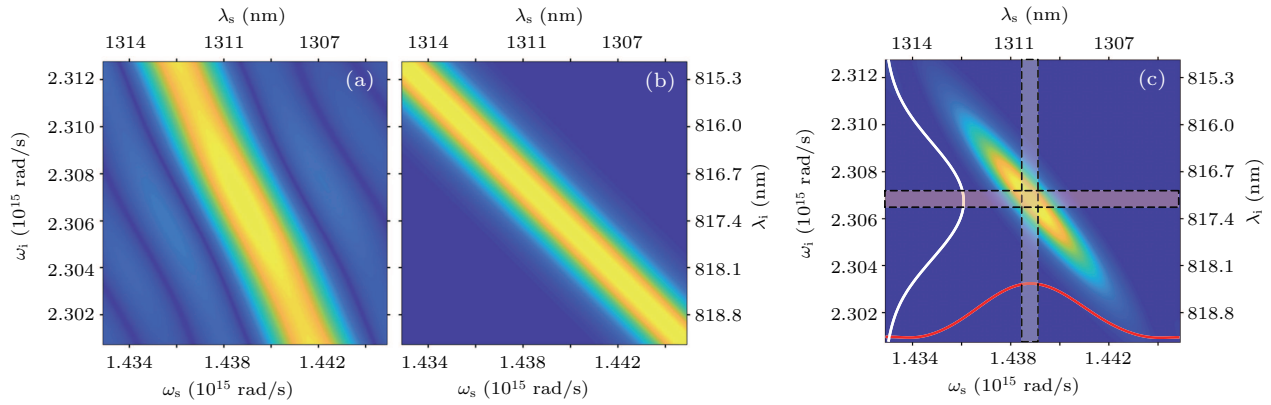


Fig. 4. Numerically simulated phase matching function (a), pump envelope function (b), and JSI (c) for SFWM biphotons in MNF. Note that frequency axes are labeled with the corresponding wavelength values.

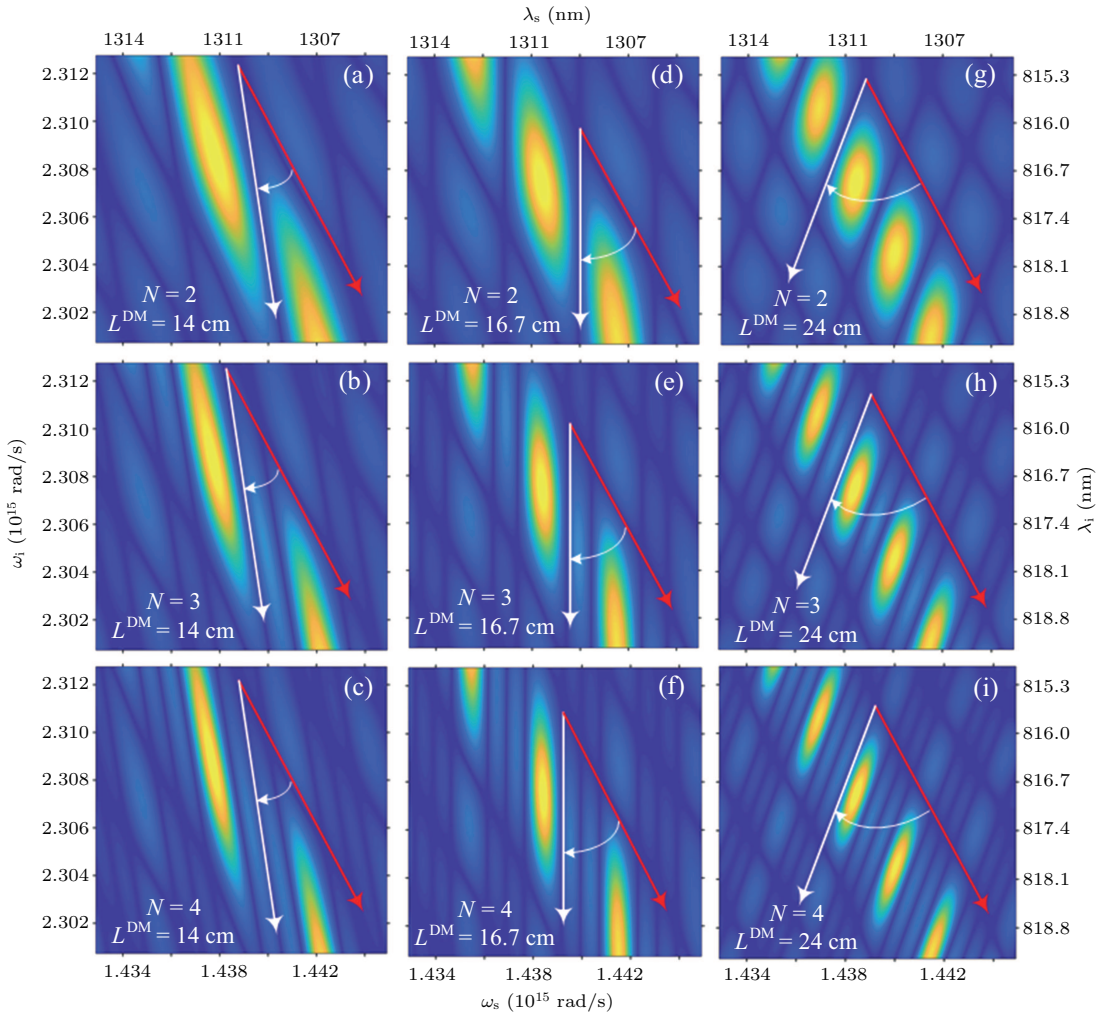


Fig. 5. Phase matching function $\mathcal{P}^{\mathrm{NLI}}(\omega_\mathrm{s},\omega_\mathrm{i})$ corresponding to stage number $N = 2$, 3, and 4, respectively, and $L^{\mathrm{DM}} = 14$ cm, 16.7 cm, and 24 cm, respectively. (a)–(c) Corresponding to negative slopes, (d)–(f) corresponding to vertical direction, and (g)–(i) corresponding to positive slopes.

Obviously, although the tapered region leads to a slight deformation in the contour of phase matching function, it can be deduced that the averages of τ_s^{NL} and τ_i^{NL}, with respect to the overall MNF in our case, are both positive numbers, i.e., $\tau_s^{NL} > 0$ and $\tau_i^{NL} > 0$. In addition, due to the conservation of energy, the orientation angle of envelope function is always $-\pi/4$. Therefore, the JSA, multiplication of Figs. 4(a) and 4(b), appears with spectrum anti-correlation, as shown in Fig. 4(c), where the contour of JSI is similar to an ellipse with the major axis having a negative slope. In Fig. 4(c), the red curve and white curve, corresponding to individual spectral distribution of signal and idler bands, respectively, have a Gaussian shape. The shadow bands represent the passive filtering with rectangle filters, which enable spectrally uncorrelated biphotons, however, in expense of reduction in brightness and weakening in heralding nature.

Equation (11) reveals the prior condition for generating factorable biphotons is GVM, i.e., $\tau_s\tau_i < 0$. Hence, the group velocity of the pump in the DMF should lie between the group velocities of the signal and idler fields. For the SFWM where $\lambda_{i0} < \lambda_{p0} < \lambda_{s0}$, GVM can be fulfilled in a common isotropic materials like silica. Here, we use single-mode communication fiber (9 μm in core radius and 0.14 in numerical aperture) as DMF to numerically simulate the rotation of phase matching contours by varying the length of DMF, as shown in Fig. 5.

In our case, $\tau_s^{NL} > 0$, $\tau_i^{NL} > 0$ and $\tau_s^{DM} > 0$, $\tau_i^{DM} < 0$, such that Fig. 5 corresponds to the first case of the fourth quadrant in Fig. 3. The red arrows and white arrows represent the orientation of phase matching contours for single MNFs ($\xi = 0$) and nonlinear interferometers ($\xi > 0$), respectively. Due to $\mathcal{P}^{NLI}(\omega_s, \omega_i) = \mathcal{P}(\omega_s, \omega_i)\mathcal{M}(\varphi)$, the interference term $\mathcal{M}(\varphi)$ modulates the single long phase matching band into periodic short strips with the same shape, and further changes the orientation angles. In this case, only if the bandwidth of $\mathcal{M}(\varphi)$ is much smaller than that of $\mathcal{P}(\omega_s, \omega_i)$, will the contours of $\mathcal{P}^{NLI}(\omega_s, \omega_i)$ significantly rotate, which can be realized by increasing the stage number N. By extending the length of DMFs, the slopes of phase matching contours vary from negative to positive. Due to the sidelobes of sinc function and vice peaks of $\mathcal{M}(\varphi)$, there are lots of dispersed disturbance cakes which will decrease the purity of single photon modes.

5. Generation spectrally uncorrelated biphotons in fiber NLI

Equation (11) reveals that only if the phase matching contours have a positive slope may spectrally uncorrelated biphotons be generated by choosing an appropriate pump bandwidth. Due to the $\mathcal{P}^{NLI}(\omega_s, \omega_i)$ contours consisting of many periodic short strips with same shape, the JSI will have a pattern of discrete ellipse. Here, we assume that the length of single-mode communication fiber is 24 cm, i.e., $L^{DM} = 24$, and $N = 2$, 3, and 4, corresponding to Figs. 5(g), 5(h), and 5(i), respectively. Then, the JSIs are shown in Fig. 6. We choose appropriate pump bandwidths to make the major axis of ellipses horizontal or vertical, indicating uncorrelation spectra. In general, we substitute linewidth for bandwidth. As for $N = 1$, 2, and 3, the linewidths are 0.7 nm, 0.35 nm, and 0.25 nm, respectively. In the cases of $N \geq 3$, there are $N - 2$ secondary ellipses between two adjacent primary ellipses, and the intensity ratio between the primary and secondary ellipses increases with the increase of N.

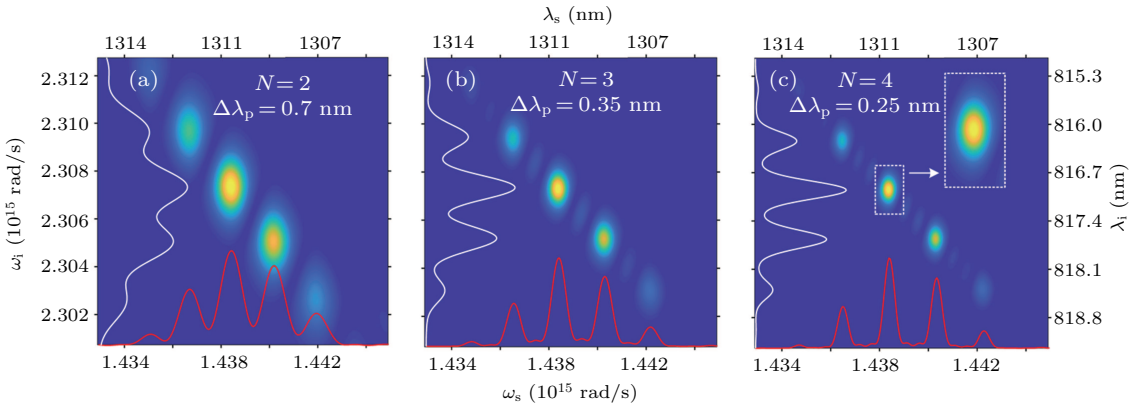


Fig. 6. JSIs of spectrally uncorrelated biphotons and individual spectral distributions of signal and idler bands. The MNF configuration is the same as that of Fig. 4. The red and white curves represent individual spectral distributions of signal and idler bands, respectively.

The marginal intensity distributions in signal and idler both have several peaks and Gaussian envelopes. Thus, in term of same filtering band, compared with filtering directly in Gaussian spectrum, filtering the center primary peak will improve the spectral brightness. Furthermore, a larger stage number, however, corresponds to a smaller ellipse, indicating a narrower bandwidth and then the central wavelengths of the primary ellipses remain unchanged. Although the spectral overlap of adjacent ellipses leads to a weak fringe visibility of marginal intensity distributions in both signal and idler bands, as shown in Fig. 6(a), the fringe visibility will significantly increase with N, as shown in Figs. 6(b) and 6(c). Therefore, we

can use passive filters in single and idler paths to extract the center primary ellipses, thus to obtain spectrally uncorrelated biphotons without weakening the heralding nature of biphoton sources. As shown in the inset of Fig. 6(c), and the mode purity is 97.2%.

Further, we can adjust the length of DMF to realize $\pi/4$ (or $-3\pi/4$) orientation angle for phase matching contours, such that the bandwidths of single and idler are equal. As shown in Fig. 7, the MNF parameters given in Fig. 4 are used as well, and $L^{\mathrm{DM}} = 43$ cm. For $N = 2$, 3, and 4, the linewidths are 0.25 nm, 0.15 nm, and 0.1 nm, respectively. Obviously, the discrete spectra have a round shape, and the marginal intensity distributions of signal and idler are the same. After passive filtering, we can obtain the spectrally uncorrelated biphotons, as shown in the inset of Fig. 7(c), and the mode purity is 96.4%.

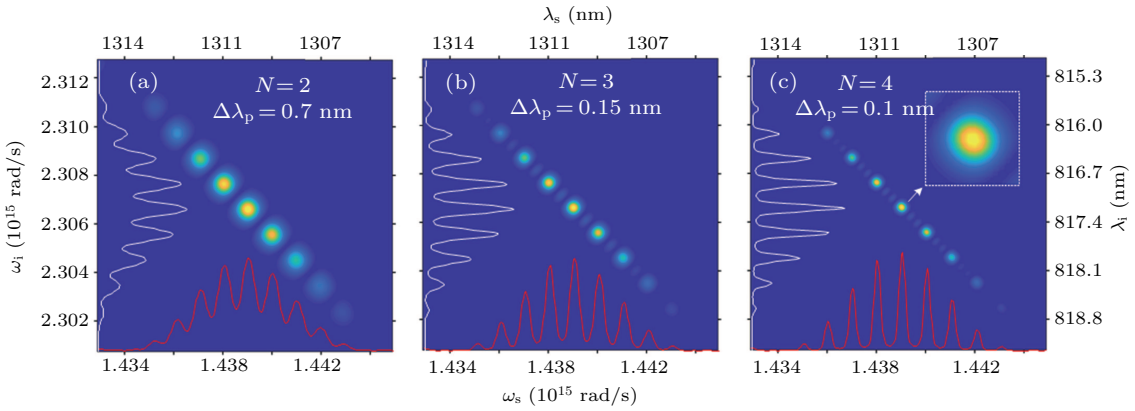


Fig. 7. JSIs of spectrally uncorrelated biphotons with a round shape. The red curve and white curve represent individual spectral distributions of signal and idler bands, respectively. The marginal intensity distributions of signal and idler are the same.

6. Conclusion

In summary, we have studied the generation of spectrally uncorrelated biphotons via fiber NLI. As for biphotons generated by spontaneous parametric emission processes, GVM crucially depends on the dispersion exhibited by the nonlinear materials and tends to occur only in specific wavelength ranges. Here, we propose a fiber NLI scheme to achieve GVM flexibly, in principle, at arbitrary phase matching wavelengths of nonlinear fiber. The output biphoton states of nonlinear interference is the coherent superposition of various biphoton states born in each NLF, and thus the interference fringe will reshape the JSI. Resorting to Taylor expansion to first order for phase mismatching, we theoretically verify that the orientation of phase matching contour will rotate in a specific way with only varying the length of DMF, which may result in an arbitrary correlation. Moreover, we choose MNF as the NLF and single-mode communication fiber as DMF to numerically simulate the phase matching contours of fiber NLI, further demonstrate that the slopes of phase matching contours vary from negative to positive by only extending the length of DMFs. The JSI will have a pattern of discrete ellipse where the intensity of center primary ellipses is the highest while the intensity of other ellipses around it decreases in Gaussian. Particularly, each discrete ellipse can be viewed as an individual JSI of biphotons. Because the spectral overlap of adjacent ellipses will significantly diminish with stage number, the passive filters can lie in single and idler path to extract the center primary ellipses, thus to obtain spectrally uncorrelated biphotons without weakening the heralding nature of biphoton sources. In our simulation, a photon mode purity of 97.2% will be theoretically attained. We think that spectrally pure biphotons generated form fiber NLI have promising application in various QIPs.

Acknowledgements

Project supported by the Science and Technology Key Project of Henan Province, China (Grant No. 182102210577), and the National Natural Science Foundation of China (Grant No. 61605249).

References

[1] Lu C Y, Cao Y, Peng C Z and Pan J W 2022 *Rev. Mod. Phys.* **94** 035001
[2] Jin R B, Wakui K, Shimizu R, Benichi H, Miki S, Yamashita T, Terai H, Wang Z, Fujiwara M and Sasaki M 2013 *Phys. Rev. A* **87** 063801
[3] Tsujimoto Y, Wakui K, Fujiwara M, Sasaki M and Takeoka M 2021 *Opt. Express* **29** 37150
[4] Valivarthi R, Puigibert Marcel li G, Zhou Q, Aguilar G H, Verma V B, Marsili F, Shaw M D, Nam S W, Oblak D and Tittel W 2016 *Nat. Photon.* **10** 676
[5] Lo H K, Curty M and Qi B 2012 *Phys. Rev. Lett.* **108** 130503
[6] Walmsley I A and Raymer M G 2005 *Science* **307** 1733
[7] Anwar A, Perumangatt C, Steinlechner F, Jennewein T and Ling A 2021 *Rev. Sci. Instrum.* **92** 041101
[8] Zhang C, Huang Y, Liu B, Li C and Guo G 2021 *Adv. Quantum Technol.* **4** 2000132
[9] Garay-Palmett K, Kim D B, Zhang Y, Domínguez-Serna F A, Lorenz V O and U'Ren A B 2022 *J. Opt. Soc. Am. B* **40** 469
[10] Garay-Palmett K, McGuinness H J, Cohen O, Lundeen J S, Rangel-Rojo R, U'ren A B, Raymer M G, McKinstrie C J, Radic S and Walmsley I A 2007 *Opt. Express* **15** 14870
[11] Mosley P J, Lundeen J S, Smith B J, Wasylczyk P, U'Ren A B, Silberhorn C and Walmsley I A 2008 *Phys. Rev. Lett.* **100** 133601
[12] Liu Y C, Guo D J, Ren K Q, Yang R, Shang M, Zhou W, Li X, Sun C W, Xu P, Xie Z, Gong Y X and Zhu S N 2021 *Sci. Rep.* **11** 12628
[13] Marhic M E, Yang F S, Min-Chen Ho and Kazovsky L G 1999 *J. Lightw. Technol.* **17** 210
[14] Cai W H, Wei B, Wang S and Jin R B 2020 *J. Opt. Soc. Am. B* **37** 3048

[15] Zhu H N, Luo B, Pan W, Yan L S, Zhao J P, Wang Z Y and Gao X R 2013 *Chin. Phys. Lett.* **30** 074206

[16] Jiang X, Zhang D, Lee T and Brambilla G 2018 *Opt. Lett.* **43** 2728

[17] Li D, Yuan C H, Ou Z Y and Zhang W 2014 *New J. Phys.* **16** 073020

[18] Marino A M, Corzo Trejo N V and Lett P D 2012 *Phys. Rev. A* **86** 023844

[19] Li J, Liu Y, Huo N, Cui L, Feng S, Li X and Ou Z Y 2020 *Phys. Rev. A* **101** 053801

[20] Kaiser F, Vergyris P, Aktas D, Babin C, Labonté L and Tanzilli S 2018 *Light Sci. Appl.* **7** 17163

[21] Lemos G B, Borish V, Cole G D, Ramelow S, Lapkiewicz R and Zeilinger A 2014 *Nature* **512** 409

[22] Riazi A, Chen C, Zhu E Y, Gladyshev A V, Kazansky P G, Sipe J E and Qian L 2019 *npj Quantum Inf.* **5** 77

[23] Su J, Cui L, Li J, Liu Y, Li X and Ou Z Y 2019 *Opt. Express* **27** 20479

[24] Li J, Su J, Cui L, Xie T, Ou Z Y and Li X 2020 *Appl. Phys. Lett.* **116** 204002

[25] Park K, Lee D and Shin H 2021 *Appl. Sci.* **11** 1429

[26] Tong L, Zi F, Guo X and Lou J 2012 *Opt. Commun.* **285** 4641

[27] Garay-Palmett K, U'Ren A B and Rangel-Rojo R 2010 *Phys. Rev. A* **82** 043809

[28] Lugani J, Francis-Jones R J A, Boutari J and Walmsley I A 2020 *Opt. Express* **28** 5147

[29] Cui L, Li X and Zhao N 2012 *New J. Phys.* **14** 123001

[30] Cui L, Su J, Li J, Liu Y, Li X and Ou Z Y 2020 *Phys. Rev. A* **102** 033718

[31] U'Ren A B, Silberhorn C, Erdmann R, Banaszek K, Grice W P, Walmsley I A and Raymer M G 2005 *Laser Physics* **15** 146

[32] U'Ren A B, Erdmann R K, de la Cruz-Gutierrez M and Walmsley I A 2006 *Phys. Rev. Lett.* **97** 223602

[33] Shukhin A A, Keloth J, Hakuta K and Kalachev A A 2020 *Phys. Rev. A* **101** 053822

[34] Kim J H, Ihn Y S, Kim Y H and Shin H 2019 *Opt. Lett.* **44** 447

[35] Kang Y, Gong J, Xu Y, Yao N, Fang W, Guo X and Tong L 2020 *IEEE Photon. Technol. Lett.* **32** 219

[36] Yao N, Linghu S, Xu Y, Zhu R, Zhou N, Gu F, Zhang L, Fang W, Ding W and Tong L 2020 *IEEE Photon. Technol. Lett.* **32** 1069

[37] Ortiz-Ricardo E, Bertoni-Ocampo C, Ibarra-Borja Z, Ramirez-Alarcon R, Cruz-Delgado D, Cruz-Ramirez H, Garay-Palmett K and U'Ren A B 2017 *Quantum Sci. Technol.* **2** 034015